Progress In Electromagnetics Research, Vol. 145, 163–173, 2014

A Compact and Wideband Circularly Polarized Rectenna with High Efficiency at X-Band

Jinwoo Shin[1], Mihui Seo[1], Junho Choi[1], Joonho So[1], and Changyul Cheon[2, *]

Abstract—A new design for a compact and wideband circularly-polarized rectenna with high efficiency operating at X-band is proposed. A dual-slot coupled antenna excited by an H-shaped slot fed by a T-shaped microstrip is designed to yield wideband performance as a receiving array antenna. Rectifying circuit models for harmonic suppression circuit, impedance matching, DC-pass circuit, and DC return circuit at the input and output of the diode are built up and optimized to transfer the maximum power from the antenna to the load using an ADS circuit simulator. An RF-DC conversion efficiency of 71.9% is measured on the conditions of 300 Ω load, and 50.1 mW RF input power at 9.5 GHz operating frequency. For the proposed wideband rectenna, the efficiency of more than 50% is measured over a 1 GHz frequency bandwidth. The measured gain, axial ratio, and return loss of the circularly polarized antenna with a 4-element array are 11.2 dBi, 1.1 dB, and −16.4 dB, respectively. The reflection coefficient of the array antenna is measured at less than −10 dB over a wide frequency range of about 2 GHz. Using this antenna as transmitting (TX) and receiving (RX) radiators, the free-space power transfer capability of the rectenna is tested in free space to turn on an LED at 25 cm distance.

1. INTRODUCTION

A rectenna, which converts RF energy to DC power, is a key component of free-space microwave power transmission (MPT) systems for the application of microwave powered unmanned aerial vehicles (UAVs) and space solar power satellite stations (SSPS) [1, 2]. The constraints on the design of MPT systems are the choice of the operating frequency and the system configuration of the transmitter and receiver. Recently, an MPT consisting of an active phased array transmitter, a rectenna array system, and a beam controlled system was tested and found to have RF to DC conversion efficiency ($\eta_{\mathrm{RF-DC}}$) of 54% at 1 mW RF input for the unit element and 5.8 GHz [3]. This system, which operated for more than 8 hours, has 256 transmitting and receiving array elements with circular polarization, allowing it to obtain a high overall $\eta_{\mathrm{RF-DC}}$.

In order to design a compact rectenna array, a high operating frequency should be chosen in order to reduce the area of the receiving array aperture. For this reason, there have been some attempts to design rectennas at 35 GHz and, 95 GHz; however, there are limitations such as lower $\eta_{\mathrm{RF-DC}}$ and higher cost to develop such high power transmitting and receiving systems [4, 5]. Therefore, there have been tradeoffs of choosing the frequency for microwave powered aerial vehicle (MPAV) systems, which operate at X-band with a compact size and light weight [6]. For the polarization diversity, compactness, and thermal management, a dual-polarized rectenna array was demonstrated at X-band to drive a high voltage actuator [7]. A low-cost planar rectenna with a FR4 substrate and a surface-mounted Schottky barrier diode was tested and found to have a low $\eta_{\mathrm{RF-DC}}$ of about 21% [8].

Figure 1 shows a general configuration of the rectenna, which consists of an antenna, a rectifying circuit, and a load. The nonlinear characteristics of diodes generate unwanted harmonic signals that

Received 28 January 2014, Accepted 8 March 2014, Scheduled 14 March 2014

* Corresponding author: Changyul Cheon (changyul@uos.ac.kr).

[1] Agency for Defense Development, South Korea. [2] University of Seoul, South Korea.

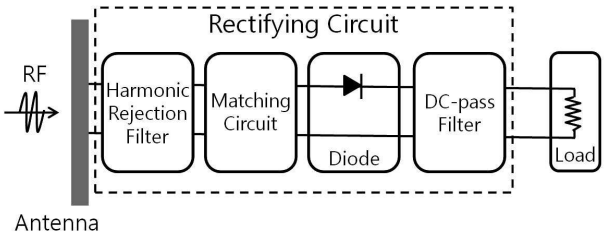

Figure 1. General configuration of a rectenna.

propagate backward to the antenna and forward to the load; therefore, a harmonic rejection filter, a DC-pass filter, and a matching circuit for the diode impedance should be carefully designed to obtain an optimized $\eta_{\mathrm{RF-DC}}$ [7–11].

This paper proposes a compact and wideband circularly-polarized (CP) rectenna operating at X-band with high $\eta_{\mathrm{RF-DC}}$. The goal of this work is to develop a wideband rectenna element while considering the frequency, polarization diversity, and large rectenna array system for MPAV applications. To obtain wideband circular polarization characteristics, a dual-slot coupled antenna excited by an H-shaped slot fed by a T-shaped microstrip was designed as the radiating element of a rectenna array. The rectifying circuit model of the rectenna is also optimized to obtain a value of $\eta_{\mathrm{RF-DC}}$ that was higher than 50% over the wide bandwidth of the X-band. In order to test and evaluate the rectenna elements, especially the rectenna circuits, 4-element transmitting and receiving TX, RX antennas were fabricated, and the power transfer capability of the rectenna with these elements was demonstrated in an experiment to turn on an LED as a load of the rectenna in the free-space.

Section 2 describes the design and measurement of the wideband CP patch antenna. Section 3 suggests optimization procedures for the RF-DC rectifying circuit to suppress out-of-band harmonics with wideband performance. Section 4 provides the test results of the proposed wideband rectenna for microwave power transfer.

2. RECEIVING ANTENNA DESIGN

2.1. Wideband CP Patch Antenna

Figure 2(a) shows the proposed receiving antenna element, which has a resonance cavity resulting from two layered square patches and foam between the patches. A vertical slot and horizontal slot provide orthogonal excitation to the cavity. The CP is achieved using a Wilkinson power divider and a delay line with a 90-degree phase difference between the two slots [12]. The patch antenna is designed to obtain broadband and CP characteristics using H-shaped slots and T-shaped feed lines that are stacked in a multi-layer substrate structure [13].

The heights of the feed line, lower patch, foam, and upper patch for each substrate are 0.38 mm, 0.64 mm, 1 mm, and 0.25 mm, respectively. The relative dielectric constants (ϵ_r) of the substrates are illustrated in Figure 2(a). In order to obtain a maximum radiation efficiency and wide bandwidth, dual patches with foam, and substrate with a low ϵ_r, are chosen, while the feed substrate has a high ϵ_r for maximum feed efficiency [14]. The resonance frequency of the cavity is mainly determined by the side length of the square patch. The sizes of the upper patch the lower patch have a small difference in order to confer the wideband characteristics of the receiving antenna element. The lengths of the upper and lower square patches are 9.64 mm and 8.51 mm, respectively.

Figure 2(b) shows the compact feeding circuits of the antenna. The T-shaped microstrip open stub occupies a small space less than that of the general microstrip open stub of length $\lambda/4$. These stubs feed the H-shaped dual slots. The Wilkinson power divider has a delay line along port 2 to create a 90-degree phase difference between the ports. Each port of the power divider has a characteristic impedance of 65 Ω instead of 50 Ω, in order to provide enough array spacing by reducing the width of the divider to raise the impedance. The optimized geometrical parameters are illustrated in Figure 2(b).

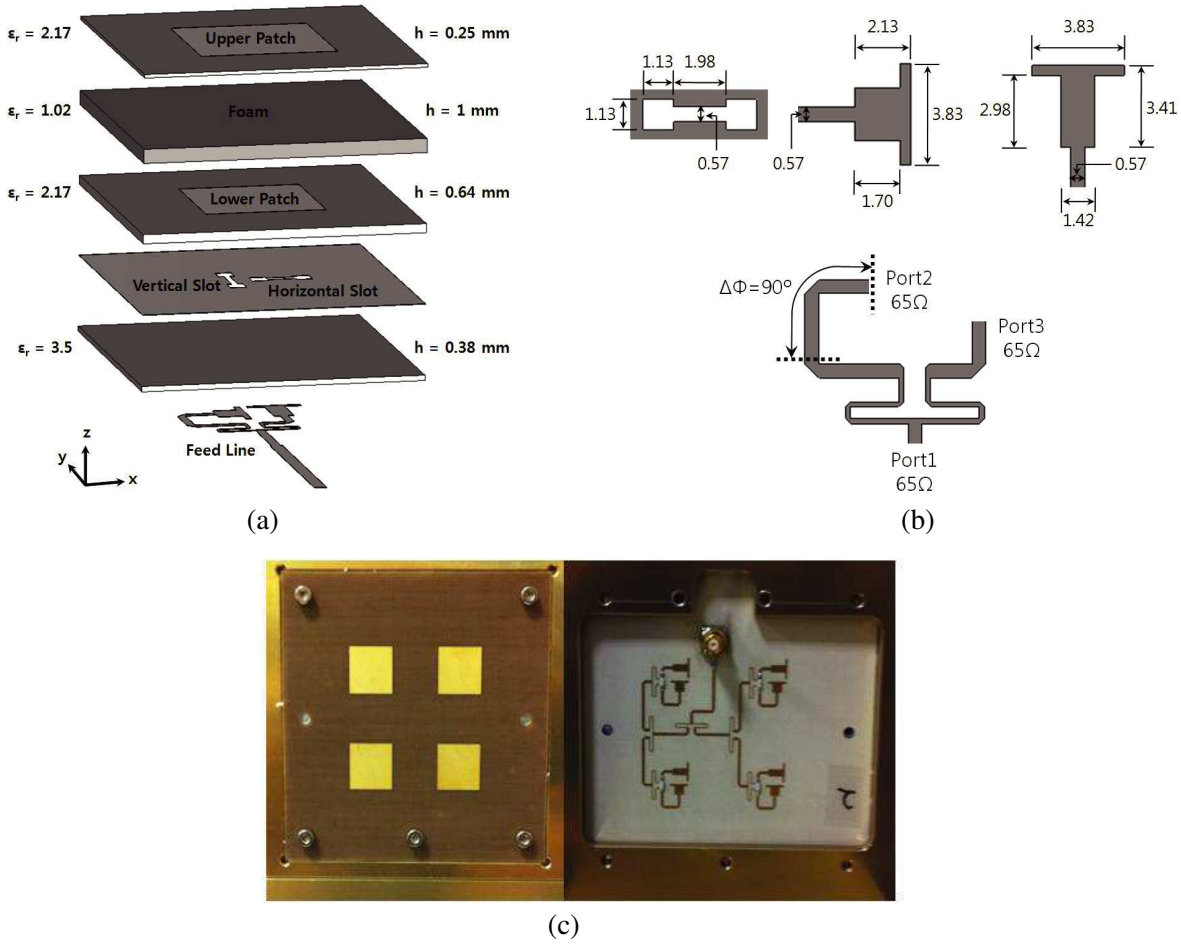

Figure 2. (a) Configuration of the CP patch antenna, (b) schematic of H-shaped slot, T-shaped feed line, and Wilkinson power divider, and (c) fabricated 4-element patch array.

Figure 2(c) shows the fabricated 4-element patch array having element spacing of 0.8λ, where λ is the wavelength at 9.5 GHz; this device has a Wilkinson power divider to feed the 4 patches. The patch cavity and microstrip feeding at the bottom-layer circuit are isolated by a conductor plane having H-shaped slots that can confer the merit of easy fabrication of the rectifier circuit on the feeding circuit layer for the large rectenna array.

2.2. Experiments for Wideband CP Patch Antenna

Figure 3(a) shows the simulated and measured reflection coefficients for the 4-element array antenna. The measured S_{11} has its lowest value at around 9.5 GHz and a wideband characteristic with less than -10 dB over the 2 GHz wideband frequency range, which is similar to the simulated frequency range. The difference of resonant frequencies in this figure is due to the PCB mount SMA connector, which is not considered during the fullwave simulation performed using CST Microwave Studio.

Figure 3(b) shows the simulated and measured gains of the fabricated 4-element patch antennas at 9.5 GHz. The horizontal radiation characteristics of the gains are shown in this figure because the patch array is symmetric, so that the vertical characteristics are similar to the horizontal characteristics. The measured gain of the 4-element antenna is in good agreement with the simulated one. The measured and simulated gains are 11.2 dBi and 12.7 dBi, respectively. The CP characteristic for the 4-element array antenna is also measured, and it is found that there is an axial ratio of 1.1 dB at the boresight angle of the antenna.

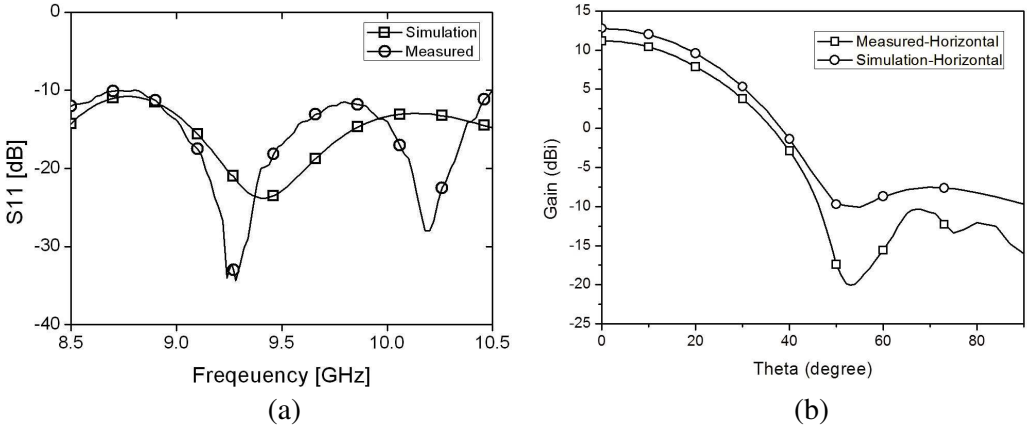

Figure 3. (a) Reflection coefficients for 4-element array antenna and (b) simulated and measured gains for 4-element array antenna.

3. RECTIFYING CIRCUIT

3.1. Design of Rectifying Circuit

The configuration of the X-band rectifying circuit is shown in Figure 4(a). The designed rectifier must be compact because a single X-band rectenna will be used for a large rectenna array application with 0.8λ element space. For this application, the feeding network of the antenna and the rectifier were designed using a microstrip line structure.

This half-wave rectifying circuit consists of a harmonic rejection filter, a matching circuit, a rectifying diode, a DC-pass filter, and a DC return. Especially, the diode is the most critical component for the high $\eta_{\mathrm{RF-DC}}$ of the rectifying circuit. The $\eta_{\mathrm{RF-DC}}$ of the rectifying circuit is defined as

$$\eta_{\mathrm{RF-DC}} = \frac{P_{\mathrm{DC}}}{P_{\mathrm{RF}}} = \frac{V_{\mathrm{DC}}^2/R_L}{P_{\mathrm{RF}}} \tag{1}$$

where P_{DC}, P_{RF}, V_{DC}, and R_L are the converted DC power, received RF power, converted DC voltage, and load impedance, respectively.

The diode of the rectenna, as shown in Figure 4(a), is the most important component in the design of a rectifying circuit and is not easy to model. Therefore, the following is considered in this paper. The diode for high $\eta_{\mathrm{RF-DC}}$ should have certain conditions such as high breakdown voltage V_{br}, which is related to the efficiency of high input power; low forward voltage V_f, which is related to the capability of

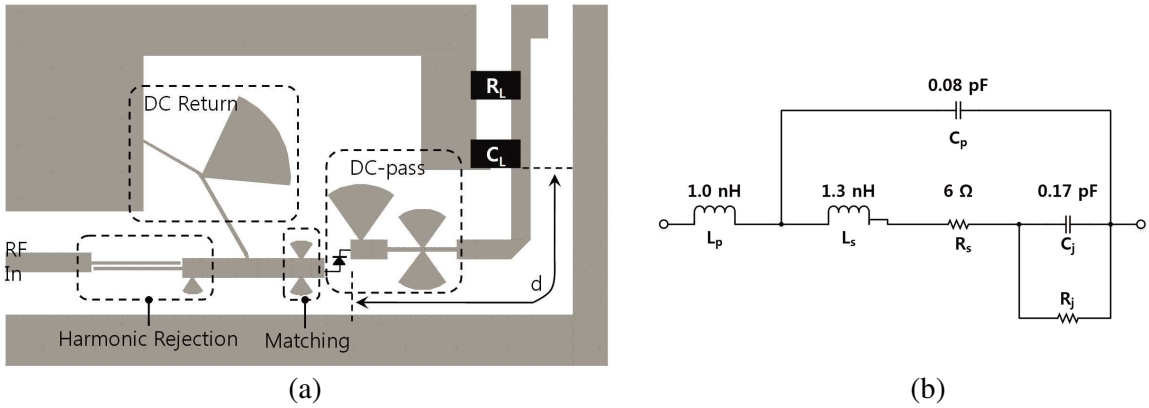

Figure 4. (a) Configuration of the designed rectifying circuit and (b) diode equivalent circuit.

capturing small signals; low series resistance R_s, which is related to the overall efficiency of the rectifier; low junction capacitance C_j, which is related to the operation bandwidth. The diode used in this paper is a packaged Schottky barrier diode of type HSMS-8101 from Avago Technologies. Since this diode operates over a frequency range from 10 GHz to 14 GHz, it is suitable for use at 9.5 GHz. According to the data sheet for this diode for the equivalent circuit, which can be seen in Figure 4(b), R_s, C_j, V_f, and V_{br} of the diode are 6 Ω, 0.17 pF, 0.25–0.35 V, and < -4 V, respectively [15], and the junction resistance R_j in this figure is variable with the operating conditions [16].

The calculated input impedance Z_{in} of the diode using ADS circuit simulation with 50 Ω source impedance is $(22 - j20)\,\Omega$ with 10 mW input power and 1000 Ω load at 9.5 GHz operating frequency. The impedance difference between the antenna and the diode causes a reduction of the power transfer and of the diode efficiency. Therefore, in order to maximize the RF power transfer from the antenna to the diode, the impedance matching circuit is designed as shown in Figure 4(a). Because Z_{in} of the diode is varied according to the operating frequency, RF input power and load resistance, the matching circuit is designed using two radial stubs for wideband operation, as shown in Figure 4(a).

Generally, the non-linearity of the diode generates higher-order harmonics, which causes the reduction of $\eta_{\mathrm{RF-DC}}$. Therefore, a harmonic rejection filter and a DC-pass filter are necessary to suppress the higher-order harmonics.

First, the harmonic rejection filter prevents the re-radiation of the RF harmonics from the diode and blocks the unwanted receiving signals from the antenna. Figure 5 shows the designed layout and S_{21} characteristics of the harmonic rejection filter at the input of the diode. The harmonic rejection filter is designed to consist of coupled microstrip lines and a radial stub. The transmission coefficient, S_{21}, is analyzed using an ADS momentum simulator. The coupled microstrip band-pass filter of the harmonic rejection filter is centered at 9.5 GHz operating frequency with −3 dB bandwidth of 7.3 GHz. And, the combined harmonic rejection filter with band-pass filter and open-circuited radial stub, which works as a band-stop filter, attenuates the first-harmonic frequency near 19 GHz and the second-harmonic frequency near 28.5 GHz in order to lower the transmission coefficient S_{21} to about −26.6 dB and −16.5 dB, respectively, as illustrated in Figure 5(b).

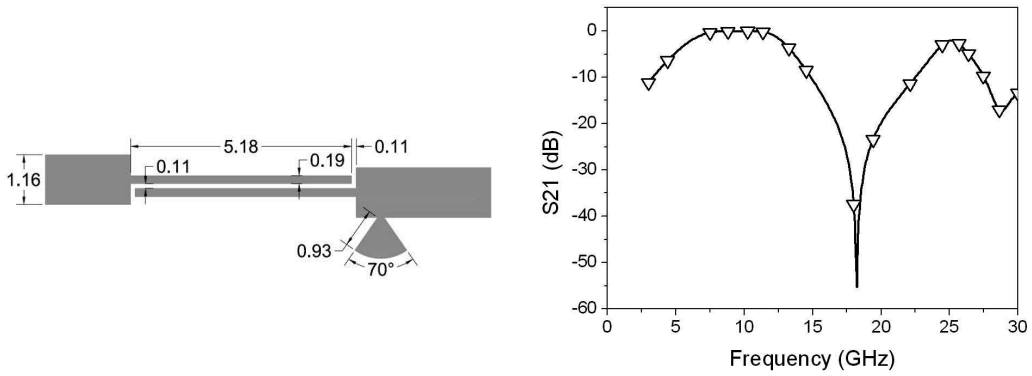

Figure 5. (a) Layout and (b) S_{21} of the input harmonic rejection filter.

Second, the DC-pass filter attenuates the RF to transmit only DC power to load. The designed layout and S_{21} characteristic of the DC-pass filter, which is positioned at the output of the diode, are given in Figure 6. The DC-pass filter with single radial stub and pair radial stubs has the function of attenuating the fundamental, the second, and the third harmonics to lower the transmission coefficient S_{21} below −15 dB. The final values of the fundamental, the second, and the third harmonics are −26 dB, −18.8 dB, and −25.5 dB, as given in Figure 6(b).

Figure 7 illustrates the DC-pass filter effect according to the distance from the diode to the capacitor (d). In the rectifying circuit, the capacitor, which is connected in parallel with the load, lowers the ripple voltage and supplies the DC power stably to the load. As shown in this figure, the DC-pass filter keeps the $\eta_{\mathrm{RF-DC}}$ almost constant with various d. On the other hand, in the case of operation without a

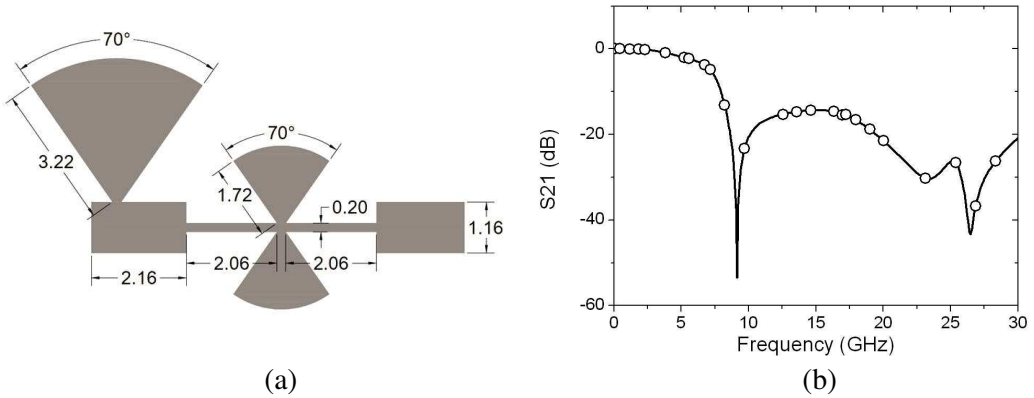

Figure 6. (a) Layout and (b) S_{21} of the DC-pass filter.

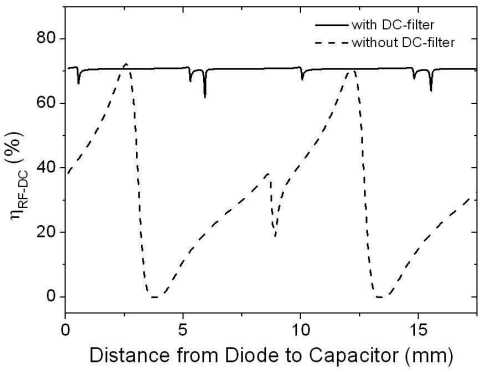

Figure 7. Efficiency according to distance from the diode to the capacitor.

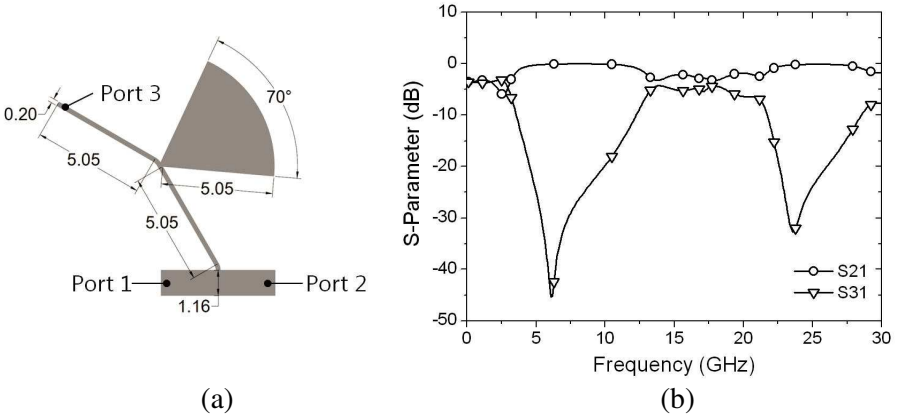

Figure 8. (a) Layout and (b) S-parameter of the DC return.

DC-pass filter, $\eta_{\mathrm{RF-DC}}$ is largely degraded, and there is an optimum length of d for the maximum $\eta_{\mathrm{RF-DC}}$ [2]. The various optimum values of d according to operation conditions cause a reduction of $\eta_{\mathrm{RF-DC}}$ with fixed d of the rectifying circuit. Therefore, the DC-pass filter is a key component for the stable operation of the rectifying circuit.

Additionally, the DC return circuit is used to reject the re-radiation of the harmonics generated by the diode when the reverse current flows into the diode. Figure 8 shows the designed layout and

S-parameter simulation results of the DC return. The DC return is used to reject the countercurrent from ground (port 3 in Figure 8(a)) to the rectifying circuit and prevent the re-radiation of RF to the antenna. The DC return functions as a band-stop filter to short out the X-band transmission between the ground (port 3) and ports 1 and 2. On the other hand, the RF transmission from port 1 to port 2 (S_{21}) at 3.2–13.5 GHz frequency (3 dB band-pass region) is not affected by the ground.

3.2. Simulation Results

The schematic model of the optimized rectifying circuit is illustrated in Figure 9; this layout corresponds to the layout of the model shown in Figure 4(a). Figures 10 and 11 show the values, calculated by harmonic balance simulation, of S_{11} and $\eta_{\mathrm{RF-DC}}$ for the estimation of the rectifying circuit performance under the various operation conditions. The $\eta_{\mathrm{RF-DC}}$ is calculated from Formula (1) with load resistance (R_L) of 50 to 1000 Ω and input powers of 10 dBm, 11 dBm, and 12.5 dBm. The rectifying circuit has been optimized with the load resistance according to the input power at 9.5 GHz operation frequency, as illustrated in Figure 10, because the diode's input impedance varies with the different operation conditions. The maximum efficiency and voltage are 71% and 2.25 V, respectively, with 12.5 dBm input power and 400 Ω load. The calculated power density of 12.5 dBm input power with RX antenna dimensions of 9.64 mm by 9.64 mm corresponds to 6.8 mW/cm^2.

Because the impedance of each rectifying circuit component and the diode varies according to the operation frequency, the development of a rectifying circuit for wideband operation is difficult. In this paper, as previously explained, the rectifying circuit components are designed using a radial stub to

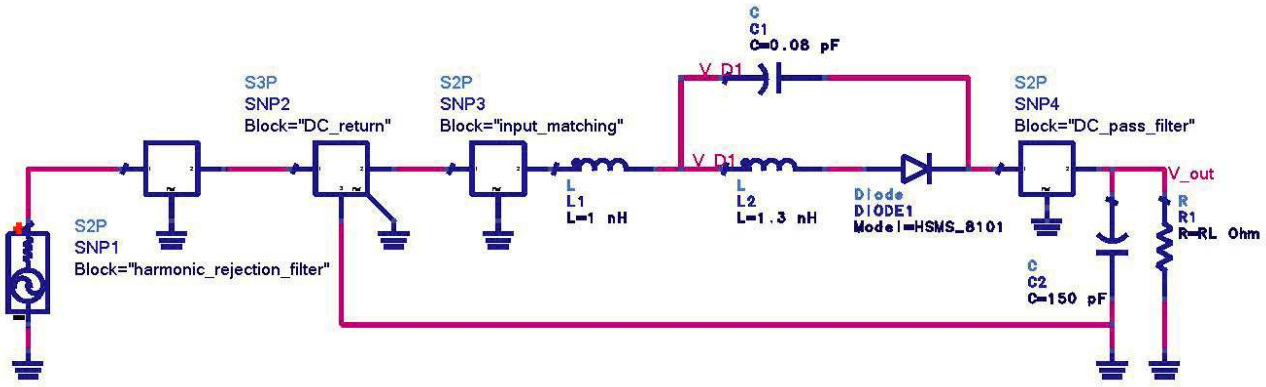

Figure 9. Simulation model of the rectifying circuit.

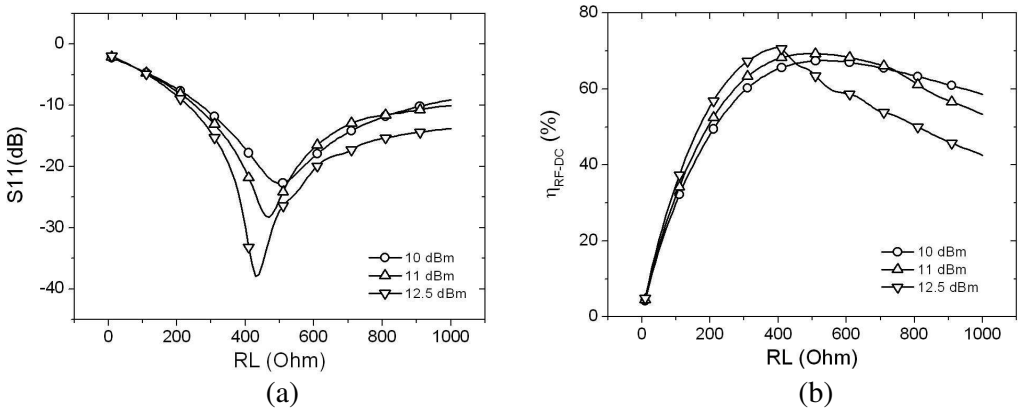

Figure 10. (a) Simulated S_{11} and (b) efficiency of the rectifying circuit according to different load and input powers at 9.5 GHz by harmonic balance simulation.

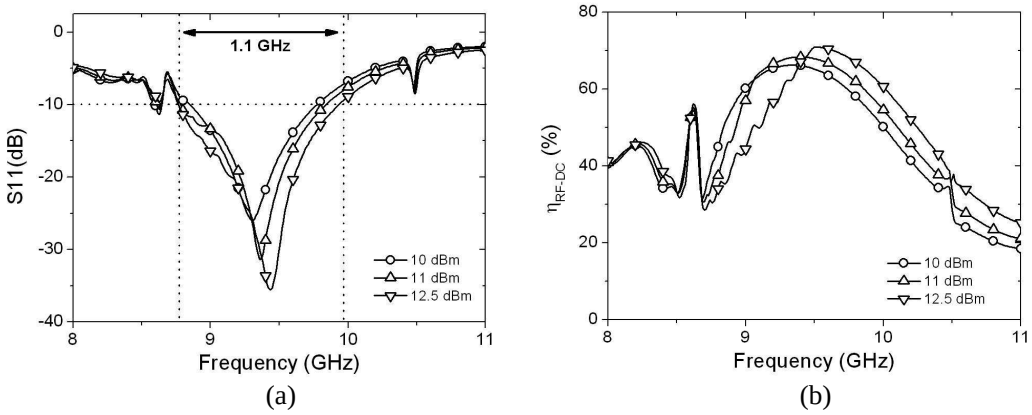

Figure 11. (a) Simulated S_{11} and (b) efficiency according to frequency and different input powers.

operate over a wideband frequency. And, the simulation results for the integrated components, shown in Figure 11, demonstrate that the designed rectifying circuit works with a value of S_{11} lower than -10 dB in the frequency range of 8.8 to 9.9 GHz. Also, $\eta_{\mathrm{RF-DC}}$ is higher than 50% in the frequency range of 9.1 to 10.2 GHz with 12.5 dBm input power.

3.3. Experimental Results for the Rectifying Circuit

The rectifying circuit was fabricated, as shown in Figure 12, on the substrate Rogers RO4003 ($\epsilon_r = 3.38$, loss tangent $\tan\delta = 0.0027$ at 10 GHz) with a thickness of 20 mil (0.508 mm). All experiments were performed with 9.5 GHz operation frequency. The capacitor is 150 pF, and a variable load is used to check the $\eta_{\mathrm{RF-DC}}$ of the rectifying circuit according to the load condition.

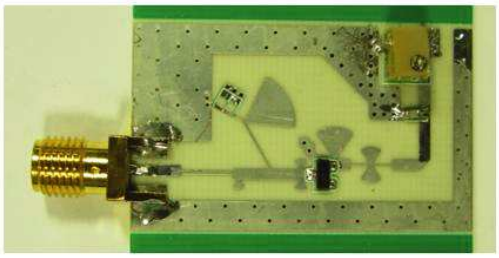

Figure 12. Fabricated rectifying circuit.

Figure 13(a) shows the measured conversion efficiency under different loads according to input powers. The tendency of the measured $\eta_{\mathrm{RF-DC}}$ according to input power and load resistance is similar to the simulation results. However, the optimum condition for the maximum $\eta_{\mathrm{RF-DC}}$ is slightly different. The simulated maximum efficiency is 71% with 12.5 dBm input power and 400 Ω load. At the same time, the measured maximum efficiency is 71.9% with 17 dBm (19.1 mW/cm^2 power density), and 300 Ω load. From the measured results, it is evident that the diode and the rectifying circuit can be used at higher input power than that estimated by ADS harmonic balance simulation with the same conversion efficiency. The converted DC voltage increases as the input power increases and the DC voltage with the maximum efficiency is 3.2 V, as can be seen in Figure 13(b).

Compared to the results for the efficiency (63.2% at 8.51 GHz [7] and 21% at 9.3 GHz [8]), the efficiency of the RF-DC conversion circuit proposed in this paper is higher than that in the papers referred to for the X-band frequency. And, the proposed rectifying circuit was measured and found to have a maximum 71.9% efficiency and more than 50% over the 1 GHz frequency range, as shown in

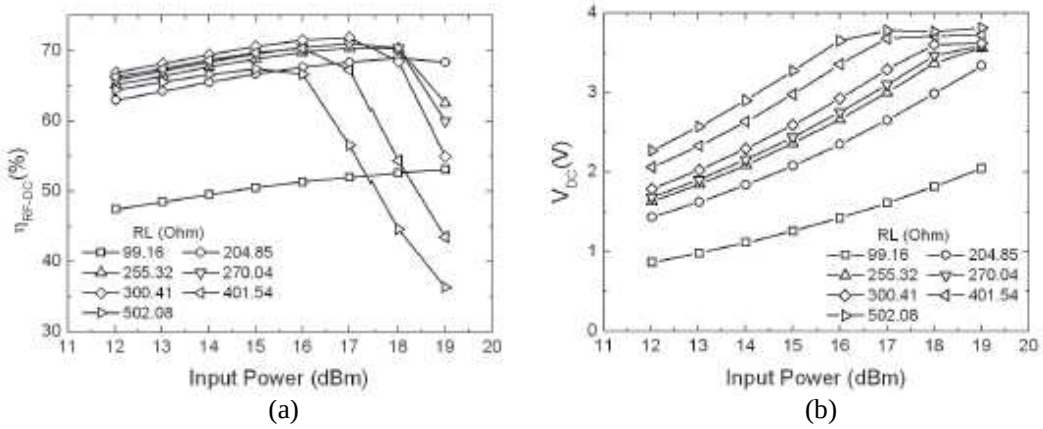

Figure 13. (a) Measured efficiency and (b) converted voltage according to input power and load.

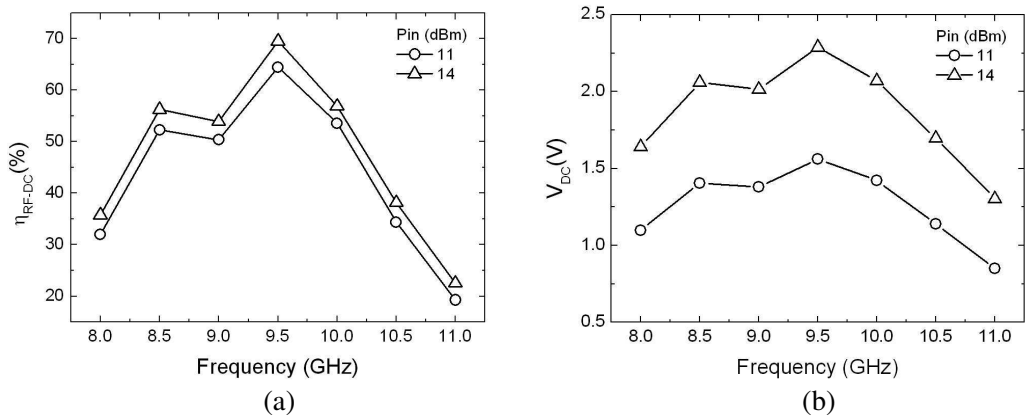

Figure 14. (a) Measured efficiency and (b) converted voltage.

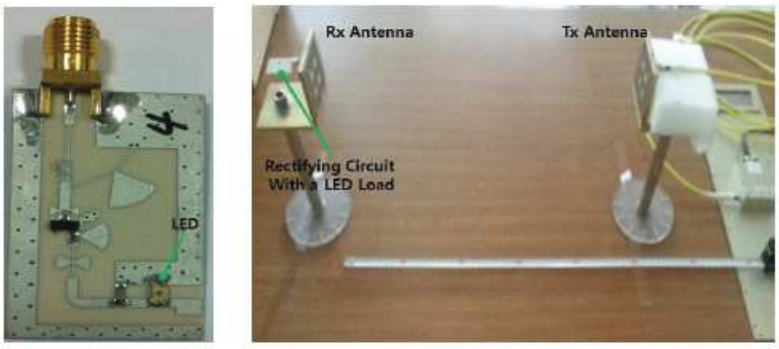

Figure 15. (a) Rectifying circuit with an LED load and (b) test setup for wireless power transfer using the designed rectenna.

Figure 14. The rectifying circuit is optimized compactly with dimensions of 35 mm by 21 mm at 9.5 GHz, making it feasible for application to the large rectenna array system. Therefore, the proposed rectenna can be applied to compact and light vehicles at X-band and can demonstrate wideband efficiency capability.

4. EXPERIMENTAL RESULTS FOR MICROWAVE POWER TRANSFER

The wideband CP antenna and the highly efficient rectifying circuit for the single rectenna were designed and fabricated individually and then connected to each other using a PCB mount SMA connector. The free-space power transfer capability of the assembled rectenna with TX and RX antennas having a 4-element patch was tested in the free space with an LED load, as shown in Figure 15(a). The TX antennas with the 4-element patch array antenna are fed by a 1 W power amplifier at 9.5 GHz, as shown in Figure 15(b). This radiating power of the TX antenna makes the LED load turn on at a distance of 25 cm when the LED impedance as a load, the input power, and the power density at the rectenna are 175 Ω, 16 mW, and 1.5 mW/cm^2, respectively. The far-field condition at the operating frequency is 32.8 cm, but the test distance is 25 cm, which is in the near-field zone. This distance is determined by considering the source power and the dynamic power range of the LED to turn on.

5. CONCLUSION

A compact and wideband rectenna circuit has been developed. This circuit has a very high conversion efficiency of 71.9% at 9.5 GHz with an input power of 50.1 mW, and it also has an efficiency of more than 50% and a frequency bandwidth of 1 GHz. The dual-slot coupled 4-patch array antenna, fed by an H-shaped slot and a T-shaped microstrip, has good measured radiation characteristics for which the gain is 11.2 dBi, axial ratio 1.1 dB, and return loss −16.4 dB. The designed antenna has a wideband characteristic of 2 GHz at X-band. The harmonic rejection, DC-pass, DC return circuits, and impedance matching circuits of the rectifying circuit were optimized using the ADS harmonic balance method and momentum solver to eliminate the harmonics and match the rectenna so as to make it not sensitive to the effects of frequency, power level, or load impedance. The free-space power transfer capability of the rectenna, with TX and RX antennas having 4-element patch tested at 25 cm distance, and the LED driven by the rectenna, turned on at a power level of 12 dBm. This compact circularly-polarized rectenna element will be applied to develop larger rectenna arrays for applications such as unmanned aircraft.

REFERENCES

1. Brown, W. C., "The history of power transmission by radio waves," *IEEE Trans. Microwave Theory Tech.*, Vol. 32, No. 9, 1230–1242, 1984.
2. Strassner, B. and K. Chang, "Microwave power transmission: Historical milestones and system components," *Proceedings of the IEEE*, Vol. 101, No. 6, 1379–1396, 2013.
3. Shinohara, N., "Power without wires," *IEEE Microwave Mag.*, S64–S73, Dec. 2011.
4. Koert, P. and J. T. Cha, "Millimeter wave technology for space power beaming," *IEEE Trans. Microwave Theory Tech.*, Vol. 40, No. 6, 1251–1258, 1992.
5. Chiou, H.-K. and I.-S. Chen, "High-efficiency dual-band on-chip rectenna for 35- and 94-GHz wireless power transmission in 0.13-μm CMOS technology," *IEEE Trans. Microwave Theory Tech.*, Vol. 58, No. 12, 3598–3606, 2010.
6. Kim, J., S.-Y. Yang, K. D. Song, S. Jones, J. R. Elliott, and I.-S. Chen, and S. H. Choi, "Microwave power transmission using a flexible rectenna for microwave-powered aerial vehicles," *Smart Mater. Struct.*, No. 15, 1243–1248, 2006.
7. Epp, L. W., A. R. Khan, H. K. Smith, and R. P. Smith, "A compact dual-polarized 8.51-GHz rectenna for high-voltage (50 V) actuator applications," *IEEE Trans. Microwave Theory Tech.*, Vol. 48, No. 1, 111–120, 2000.
8. Monti, G., L. Tarricone, and M. Spartano, "X-band planar rectenna," *IEEE Antennas Wireless Propagat. Lett.*, Vol. 10, 1116–1119, 2011.
9. Yang, X.-X., C. Jiang, A. Z. Elsherbeni, F. Yang, and Y.-Q. Wang, "A novel compact printed rectenna for data communication systems," *IEEE Trans. Antennas Propagat.*, Vol. 61, No. 5, 2532–2539, 2013.

10. Gao, Y.-Y., X.-X. Yang, C. Jiang, and J.-Y. Zhou, "A circularly polarized rectenna with low profile for wireless power transmission," *Progress In Electromagnetics Research Letters*, Vol. 13, 41–49, 2010.
11. Kim, P., G. Chaudhary, and Y. Jeong, "A dual-band RF energy harvesting using frequency limited dual-band impedance matching," *Progress In Electromagnetics Research*, Vol. 141, 443–461, 2013.
12. Gao, S. and A. Sambell, "Low-cost dual-polarized printed array with broad bandwidth," *IEEE Trans. Antennas Propagat.*, Vol. 52, No. 12, 3394–3397, 2004.
13. Ravipati, C. B. and L. Shafai, "A wide bandwidth circularly polarized microstrip antenna using a single feed," *IEEE AP-S Int. Symp. Dig.*, Vol. 1, 244–247, 1999.
14. Kirov, G. S. and D. P. Mihaylova, "Circularly polarized aperture coupled microstrip antenna with resonant slots and a screen," *Radioengineering*, Vol. 19, No. 1, 111–116, 2010.
15. Surface Mount Microwave Schottky Mixer Diodes, HSMS-8101, 8202, 8207, 8209 Series Avago Technologies, 2009.
16. Hansen, J. and K. Chang, "Diode modeling for rectenna design," *Proc. of 2011 IEEE APSURSI Int. Symp.*, 1077–1080, 2011.